Myosin II directly binds and inhibits Dbl family guanine nucleotide exchange factors: a possible link to Rho family GTPases

Chan-Soo Lee,[1] Chang-Ki Choi,[1] Eun-Young Shin,[1] Martin Alexander Schwartz,[2] and Eung-Gook Kim[1]

[1]Department of Biochemistry and Medical Research Center, Chungbuk National University College of Medicine, Cheongju 361-763, South Korea
[2]Departments of Microbiology, Cell Biology, and Biomedical Engineering, Robert M. Berne Cardiovascular Research Center, Mellon Prostate Cancer Research Center, University of Virginia, Charlottesville, VA 22908

Cell migration requires the coordinated spatiotemporal regulation of actomyosin contraction and cell protrusion/adhesion. Nonmuscle myosin II (MII) controls Rac1 and Cdc42 activation, and cell protrusion and focal complex formation in migrating cells. However, these mechanisms are poorly understood. Here, we show that MII interacts specifically with multiple Dbl family guanine nucleotide exchange factors (GEFs). Binding is mediated by the conserved tandem Dbl homology–pleckstrin homology module, the catalytic site of these GEFs, with dissociation constants of ~0.3 μM. Binding to the GEFs required assembly of the MII into filaments and actin-stimulated ATPase activity. Binding of MII suppressed GEF activity. Accordingly, inhibition of MII ATPase activity caused release of GEFs and activation of Rho GTPases. Depletion of βPIX GEF in migrating NIH3T3 fibroblasts suppressed lamellipodial protrusions and focal complex formation induced by MII inhibition. The results elucidate a functional link between MII and Rac1/Cdc42 GTPases, which may regulate protrusion/adhesion dynamics in migrating cells.

Introduction

Nonmuscle myosin II (MII) contractility is critically important in cell motility (Vicente-Manzanares et al., 2007). MII contains pairs of myosin heavy chains (MHCs), regulatory myosin light chains (MLCs), and essential MLCs that assemble into bipolar filaments with actin-stimulated ATPase activity. The resultant contractility drives formation of actin stress fibers and focal adhesions. MII also cross-links actin, which contributes to adhesion assembly and stabilization of actin filaments (Choi et al., 2008). Although MII is located away from the lamellipodium and nascent adhesions (Kolega, 1998, 2006; Gupton and Waterman-Storer, 2006), its removal or inhibition induces ectopic lamellipodia and adhesions (Katsumi et al., 2002; Sandquist et al., 2006; Even-Ram et al., 2007; Vicente-Manzanares et al., 2007). MII might therefore control a diffusible factor(s) that affects processes at the leading edge.

Rac1, Cdc42, and RhoA jointly control lamellipodial and filopodial protrusions, adhesion dynamics, and actin stress fibers during migration (Nobes and Hall, 1995). Rho GTPases regulate MII through multiple pathways (Somlyo and Somlyo, 2000). In general, RhoA/Rho-kinase (ROCK) activates MII contractility whereas Rac1 and its effector PAK often negatively regulate MII and decrease contractility. Efficient cell motility requires that Rac1/Cdc42, RhoA, and MII activity be coordinated; however, the mechanisms of coordination remain incompletely understood.

Rho GTPases are activated by guanine nucleotide exchange factors (GEFs), most of which contain a tandem Dbl homology (DH)–pleckstrin homology (PH) domain as a catalytic core (Schmidt and Hall, 2002). Recent studies have revealed a connection between MII and Dbl family GEFs, suggesting their potential regulation by MII as well as a scaffold function (Wu et al., 2006; Conti and Adelstein, 2008). However, the molecular

Correspondence to Eung-Gook Kim: egkim@chungbuk.ac.kr; or Eun-Young Shin: eyshin@chungbuk.ac.kr

Abbreviations used in this paper: BBS, blebbistatin; DH, Dbl homology; GEF, guanine nucleotide exchange factor; HMM, heavy meromyosin; IP, immunoprecipitation; MHC, myosin heavy chain; MII, nonmuscle myosin II; MLC, myosin light chain; PH, pleckstrin homology; ROCK, RhoA/Rho-kinase.

The Rockefeller University Press $30.00
J. Cell Biol. Vol. 190 No. 4 663–674
www.jcb.org/cgi/doi/10.1083/jcb.201003057

mechanism is unknown. We therefore investigated how MII might regulate GEFs for Rho GTPases. Our studies reveal that MII regulates multiple Dbl family members through direct binding, which controls their activity and localization in migrating cells.

Results

Identification of βPIX GEF as a novel MII-interacting protein

To test whether MII regulates Rho GTPases through Dbl family GEFs, we first examined whether MII could associate with βPIX, a Rac1/Cdc42-specific GEF highly implicated in cell motility (Za et al., 2006). PC12 cells express βPIX and MIIA/MIIB at high levels, so they were used for most immunoprecipitation (IP) experiments on this GEF. βPIX IPs in PC12 cells contained MIIA and MIIB, whereas nonimmune IPs showed no association (Fig. 1 A). To test the specificity of the interaction, we screened Jurkat T cells and C2C12 myoblasts that expressed MIB and MVa, respectively (Fig. 1 A). No interaction between βPIX and myosin IB, Va, or VI was detected, indicating that the MII–βPIX interaction is specific (Fig. 1 A).

To identify the domain(s) involved in the βPIX–MII interaction, multiple MIIB and βPIX constructs were examined (Fig. 1, B and C, top). MIIB constructs were tagged with GFP and expressed in PC12 cells. IP with anti-GFP antibody followed by immunoblotting for endogenous βPIX showed that the MII head domain bound βPIX (Fig. 1 B, bottom). Conversely, analysis of βPIX constructs showed that only the N terminus of βPIX associated with MIIB (Fig. 1 C, bottom left). Further analysis revealed the DH domain as the MIIB interaction site (Fig. 1 C, bottom right). To confirm these results, the βPIX DH domain was overexpressed as GST-tagged proteins. Addition of this domain to cell lysates blocked coIP of MIIB and βPIX, whereas GST alone or βPIX SH3 domain had no effects (Fig. 1 D).

MII directly interacts and colocalizes with the Dbl family of GEFs

The high conservation of the DH domain led us to test whether other Dbl family GEFs also bind MII. We therefore expressed myc-tagged GEFs and tested for association with endogenous MIIB (Fig. 2 A). MIIB was present in IPs of all of the Dbl family of GEFs tested, but not with ARNO or smgGDS, which are GEFs that lack DH domains. Next, we examined the interaction between endogenous MII and GEFs. In rat brain lysate, the GEFs kalirin, FGD1, and LARG were readily detected (Fig. 2 B, top left), whereas PC12 cells expressed βPIX and Tiam1 (Fig. 2 B, top center) and NIH3T3 cells expressed GEF-H1, Dbl, and Trio (Fig. 2 B, top right). IP of MIIB revealed association with all of these GEFs to varying extents. When quantified by densitometry, the percentage of GEFs present in MII IPs varied from nearly 9 to ∼1% (Trio, 8.7%; GEF-H1, 8.2%; FGD1, 8.1%; Kalirin, 5.6%; βPIX, 3.0%; LARG, 1%; Dbl, 1.3%; Tiam1, 1.6%). We also compared MIIA to MIIB. The amounts of βPIX and Trio in MIIA IPs were 3.5% and 10.7%, respectively (Fig. 2 B, bottom). However, GEF-H1 decreased to 2.6% compared with 8.2% for MIIB IPs. Thus, some quantitative differences were observed.

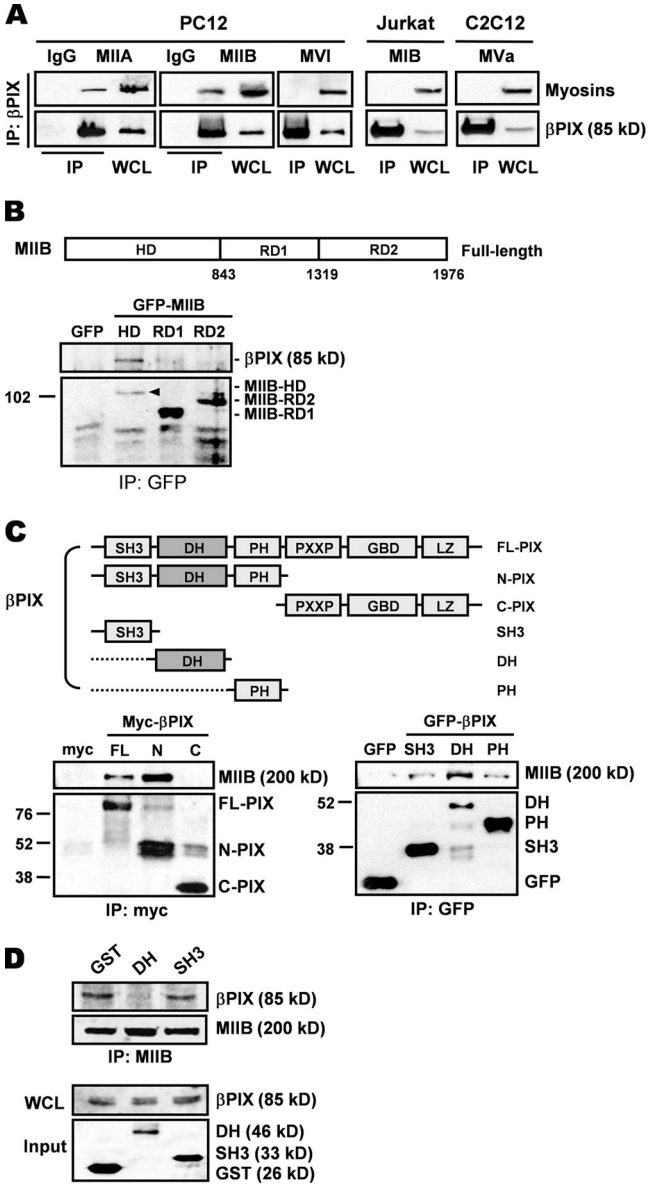

Figure 1. **Identification and characterization of interaction between MII and βPIX.** (A) Specific interaction of MII with βPIX. Cell lysates were immunoprecipitated with anti-βPIX antibody followed by immunoblotting for the indicated myosins (top). Blots were reprobed for βPIX (bottom). (B) The MIIB head domain as the binding site. Schematic diagram of the MIIB constructs (top). Cells were transfected with plasmids for the indicated MIIB constructs (bottom). Lysates were immunoprecipitated with anti-GFP antibody and immunoblotted for GFP or βPIX. (C) DH domain of βPIX as the binding site. Schematic diagram of the domain structure of βPIX (top). Full-length βPIX (FL-PIX), N-terminal βPIX (N-PIX), or C-terminal βPIX (C-PIX) were expressed as myc-tagged proteins. The SH3, DH, or PH domains were expressed as GFP fusion proteins. Cells were transfected with plasmids for the indicated βPIX constructs (bottom). Lysates were immunoprecipitated with anti-myc (left) or anti-GFP (right) antibodies and immunoblotted for MIIB or myc/GFP-tagged proteins. (D) Blocking the interaction between endogenous MIIB and βPIX with recombinant proteins. The DH domain of βPIX (DH) and the βPIX SH3 domains were expressed in *Escherichia coli* as GST-tagged proteins and purified. Cell lysates were immunoprecipitated for MIIB (top) in the presence of the 5 µg recombinant proteins. Interactions were monitored by immunoblotting for βPIX. Loading of βPIX from the lysates and the recombinant proteins were verified (bottom). Blots are representative of three independent experiments.

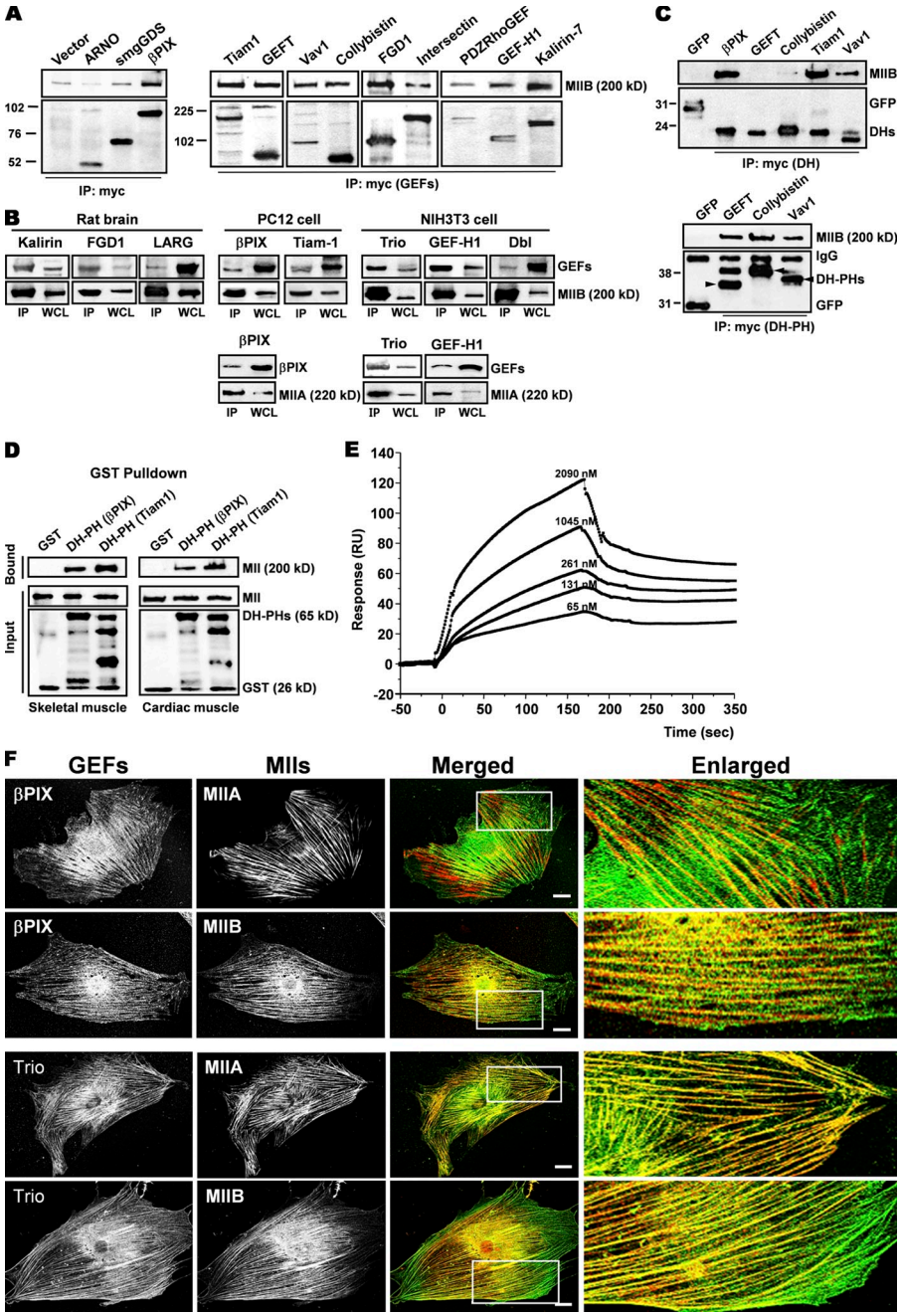

Figure 2. **Direct interaction and colocalization of MII with GEFs.** (A) Specific interaction of endogenous MIIB with ectopically expressed Dbl family GEFs. PC12 cells were transfected with myc-tagged GEFs (right), or with ARNO or smgGDS GEF, which lacks a DH domain (left). Cell lysates were immunoprecipitated with anti-myc antibody followed by immunoblotting for MIIB (top). Expression of transfected genes was verified with anti-myc antibody (bottom). (B) Quantification of interactions between endogenous MIIA/MIIB and GEFs. Lysates (1 mg) from rat brain (E18), PC12, or NIH3T3 cells were immunoprecipitated with anti-MIIA or MIIB antibody followed by immunoblotting for the indicated GEFs. All of the immunoprecipitated proteins were loaded in each IP lane. A fraction (30 μg) of the same lysates for IP was loaded in each WCL lane. The percentage of each MII-bound GEF was calculated from dividing the relative densitometric values from the IP lane by those from the paired WCL lane. (C) Involvement of the DH–PH domain in interactions with MIIB. (Top) Myc-tagged GFP (control) or the DH domains from the various GEFs were expressed in PC12 cells. Lysates were immunoprecipitated with anti-myc antibody and immunoblotted for MIIB. (Bottom) Myc-tagged DH–PH domains from GEFT, collybistin, or Vav1 (positive control) were expressed and lysates were processed as described above. (D) Direct interaction of MII with DH–PH domains. Purified recombinant GST–DH–PH domains (2 μg) were incubated with MII (1 μg) from skeletal or cardiac muscle, then precipitated with glutathione agarose beads. Bound material was analyzed by immunoblotting for skeletal or cardiac MII. (E) Binding sensorgrams for the DH–PH domain and MII. His-tagged C-PIX (control, see Fig. 1 C) or DH–PH domain were immobilized on a Ni^{2+}-NTA sensor chip and MII was passed over the immobilized proteins. Surface plasmon resonance was recorded and nonspecific binding of MII with C-PIX was subtracted from each DH–PH binding curve. (F) Colocalization of MIIs and GEFs. Swiss 3T3 cells were serum starved overnight and costained for βPIX (green) and MIIA/MIIB (red) (top), and for Trio (green) and MIIA/MIIB (red) (bottom). Enlarged images are shown on the right. Data are representative of three independent experiments. Bar, 10 μm.

As the βPIX DH domain alone showed substantial binding to MIIB (Fig. 1 C), the potential involvement of other DH domains was assessed. Myc-tagged βPIX DH domain consistently bound MIIB (Fig. 2 C, left). DH domains from Tiam1 and Vav1 also coimmunoprecipitated with MIIB, whereas those from GEFT and collybistin did not. However, DH–PH modules from GEFT and collybistin efficiently associated with MIIB (Fig. 2 C, right), whereas GFP alone did not. Thus, the DH–PH module or, in some cases, the DH domain alone, mediates MIIB binding.

To determine whether binding was direct, in vitro binding analyses used purified MIIs from skeletal and cardiac muscle, together with recombinant GST-tagged βPIX and Tiam1 DH–PH domains. Human muscle and nonmuscle MII are overall 60–62% similar, which rises to 68% at their head domains. Both skeletal and cardiac muscle MII bound to the DH–PH domains (Fig. 2 D). Thus, interactions with GEFs are direct and extend to all MII isoforms.

We next measured binding affinity using a Biacore system. Varying concentrations of MII were applied to GST (control) or GST–DH–PH immobilized on chips. Specific binding between the βPIX DH–PH domain and MII was observed after subtraction of nonspecific GST binding. The calculated K_D was 0.26 μM (Fig. 2 E). The DH–PH domains from Tiam1 and Vav1 showed similar K_D values of 0.29 and 0.39 μM, respectively (not depicted). Given the micromolar concentrations of MII in cells, these K_D values suggest that a substantial fraction of GEFs could be bound to myosin in cells.

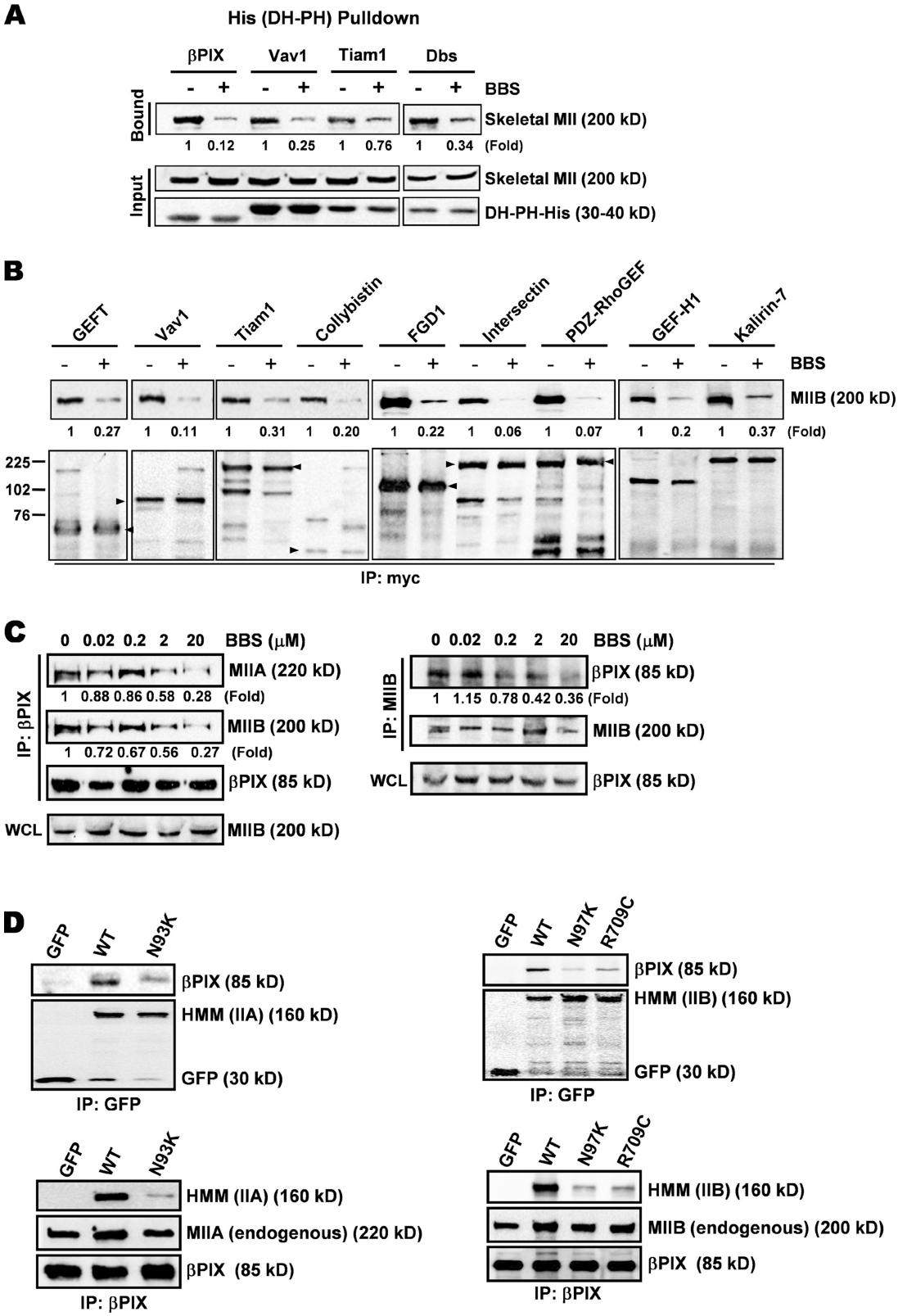

Figure 3. **MII ATPase activity critically regulates MII–GEF association.** (A) BBS-induced dissociation of the MII–DH–PH complex in vitro. Skeletal muscle MII (1 μg) was incubated with His-tagged DH–PH domains (5 μg) from βPIX, Vav1, Tiam1, or Dbs, with or without 50 μM BBS at 25°C for 30 min, followed by precipitation with Ni^{2+} beads. Bound MII was detected by immunoblotting and analyzed by densitometry. Numbers indicate binding relative to BBS-untreated lanes. (B) BBS-induced dissociation of the MII–GEF complex in cells. Various myc-tagged GEFs were expressed in 293T cells and treated with DMSO (control) or 20 μM BBS for 1 h. Lysates (1 mg) were immunoprecipitated with anti-myc antibody and immunoblotted for MIIB (top) or myc (bottom). Bands were quantified by densitometry. The results are expressed as band intensity relative to untreated samples and shown below the band of each GEF. (C) Dose-dependence for BBS. PC12 cells were incubated with the indicated concentrations of BBS for 1 h. Lysates were then immunoprecipitated with

Next, subcellular colocalization of MII and GEFs was examined. PC12 cells do not spread well and have less well-defined cytoskeletal compartments; thus, we used two 3T3 cell lines for this study. In Swiss 3T3 fibroblasts, MII stains actin stress fibers, as expected. βPIX colocalized with both MIIA and MIIB along the stress fibers, in addition to staining of elongated puncta at the end of stress fibers, consistent with its known focal adhesion localization (Manser et al., 1998), and some diffuse cytosolic staining (Fig. 2 F, top). Exogenously introduced myc-βPIX showed a similar linear localization along the stress fibers (Fig. S1). The neuronal GEF Trio has not previously been investigated in nonneuronal cells, but in fibroblasts we observed striking appearance along the stress fibers (Fig. 2 F, bottom). Merged images showed substantial colocalization for both βPIX/MII and Trio/MII, which was stronger for Trio/MII, in correlation with more efficient coIP (Fig. 2 B). Similar colocalization of these GEFs was observed in NIH3T3 fibroblasts, though stress fibers were less prominent than in Swiss 3T3s (Fig. S2).

MII ATPase activity is required for association of MII with GEFs

MII is an actin-based molecular motor that requires ATPase activity to generate contractile force. To investigate the role for ATPase activity in the GEF interaction, we used blebbistatin (BBS), which specifically inhibits ATPase activity (Straight et al., 2003; Kovács et al., 2004). BBS significantly attenuated the association of DH–PH domains from βPIX, Vav1, Tiam1, and Dbs with skeletal muscle MII (Fig. 3 A). Similar results were obtained using full-length GEFs expressed in 293T cells, which transfect efficiently (Fig. 3 B). Densitometry revealed that inhibition ranged from 94% for intersectin to the 63% for kalirin-7. Binding of endogenous βPIX to MIIA and IIB was inhibited by BBS in a dose-dependent manner, revealed by IP of both βPIX (Fig. 3 C, left) and MIIB (Fig. 3 C, right).

To confirm these results, we analyzed ATPase-defective MII heavy chain mutants: MIIA N93K, MIIB N97K, and MIIB R709C. These mutants displayed ∼4%, 70%, and 29%, respectively, of the maximal actin-activated ATPase activity of the wild type in vitro (Hu et al., 2002; Kim et al., 2005). To enhance expression levels, these mutants were expressed in 293T cells as heavy meromyosin (HMM), composed of a globular head domain, neck region, and a small fragment of the tail. The MIIA N93K, MIIB N97K, and MIIB R709C mutants bound much less βPIX compared with WT MII (Fig. 3 D, top). Reciprocal IP of βPIX gave similar results (Fig. 3 D, bottom). Thus, MII ATPase activity is required for its association with GEFs.

MLC phosphorylation and actomyosin assembly facilitates GEF binding to MII

MII assembly into thick filaments and ATPase activity are regulated by MLC phosphorylation (Adelstein and Conti, 1975), which is controlled in cells by ROCK and MLCK (Gallagher et al., 1991). Both the specific MLCK inhibitor ML-7 and the ROCK inhibitor Y-27632 decrease MII ATPase activity. We found that these inhibitors disrupted the MII–βPIX complex in a dose-dependent manner (Fig. S3, A and B). Inhibition of the RhoA/ROCK pathway with dominant-negative N19RhoA also significantly reduced coIP of MIIB-βPIX, whereas GFP or GFP-active V14RhoA had no effect (Fig. 4 A). Cellular ATP depletion can also inactivate MII, most likely through the down-regulation of RhoA/ROCK activity (Raman and Atkinson, 1999). Depleting ATP with antimycin A, an inhibitor of the complex III in the mitochondrial respiratory chain (Canfield et al., 1991), resulted in time- and dose-dependent inhibition of MIIB–βPIX coIP (Fig. 4 B). ATP depletion also inhibited MII binding to GEFT, Vav1, Tiam1, and GEF-H1 (Fig. S3 C). These data show that reducing MLC phosphorylation decreased the interaction with GEFs.

MII ATPase activity is stimulated by F-actin and requires MII assembly into thick filaments. Prominent association of βPIX/Trio with MII along the actin stress fibers suggests that assembled, active MII filaments mediate the association with GEFs (Fig. 2 F and Fig. S1). To test this idea, we addressed whether F-actin affects the formation of MII–GEF complex in vitro. Based on the finding that DH–PH domain bound to MII (Fig. 2, D and E), recombinant DH–PH domains from βPIX, Tiam1, or Vav1 were incubated with skeletal muscle MII in the absence or presence of F-actin. Because the C-terminal half of βPIX (C-PIX) does not bind MII (Fig. 1 C), it was used as a negative control. C-PIX showed a low level of binding, which was not affected by F-actin (Fig. 4 C, left). In contrast, F-actin stimulated the association of the DH–PH domains with MII by two- to fourfold. To test the importance of F-actin for this interaction in cells, they were treated with cytochalasin D, which reduces levels of F-actin. Compared with vehicle (DMSO), cytochalasin D decreased coIP of MIIB with βPIX, though less efficiently than BBS (Fig. 4 C, right).

Next, we compared full-length MII to soluble HMM, which cannot polymerize due to deletion of the C terminus. Soluble HMM bound to βPIX DH–PH domain in vitro less well than full-length MII (Fig. 4 D). To address this issue in cells, assembled MII was separated from soluble MII by mild detergent extraction (0.5% Triton X-100 in low salt with Mg^{2+}, first fraction); the pellets were then solubilized using harsher buffer (1% Triton X-100 in high salt without Mg^{2+}, second fraction) to retrieve assembled MII. Approximately 90% of the MIIA and 60% of the MIIB were in the first fraction (Fig. 4 E, left), similar to previous results from A549 cells (Sandquist and Means, 2008). We therefore concentrated on MIIB, which was more evenly distributed. Both pools were then subject to

an anti-βPIX (left) or anti-MIIB (right) antibody. Interactions were detected by immunoblotting for MIIA, MIIB, or βPIX. Bound MII or βPIX was analyzed by densitometry and the results are expressed relative to BBS-untreated control. (D) Analysis of βPIX binding by ATPase activity–deficient MIIs. (Left) GFP-tagged wild type or mutant (N93K) of MIIA HMM was expressed in 293T cells. Lysates were immunoprecipitated with anti-GFP (top) or anti-βPIX (bottom) followed by immunoblotting for βPIX, GFP for HMM constructs, or MIIA. (Right) GFP-tagged wild type or mutant (N97K/R709C) of MIIB HMM was expressed in 293T cells. Lysates were immunoprecipitated with anti-GFP (top) or anti-βPIX (bottom) followed by detection for βPIX, GFP for HMM constructs, or MIIB. Blots are representative of three independent experiments.

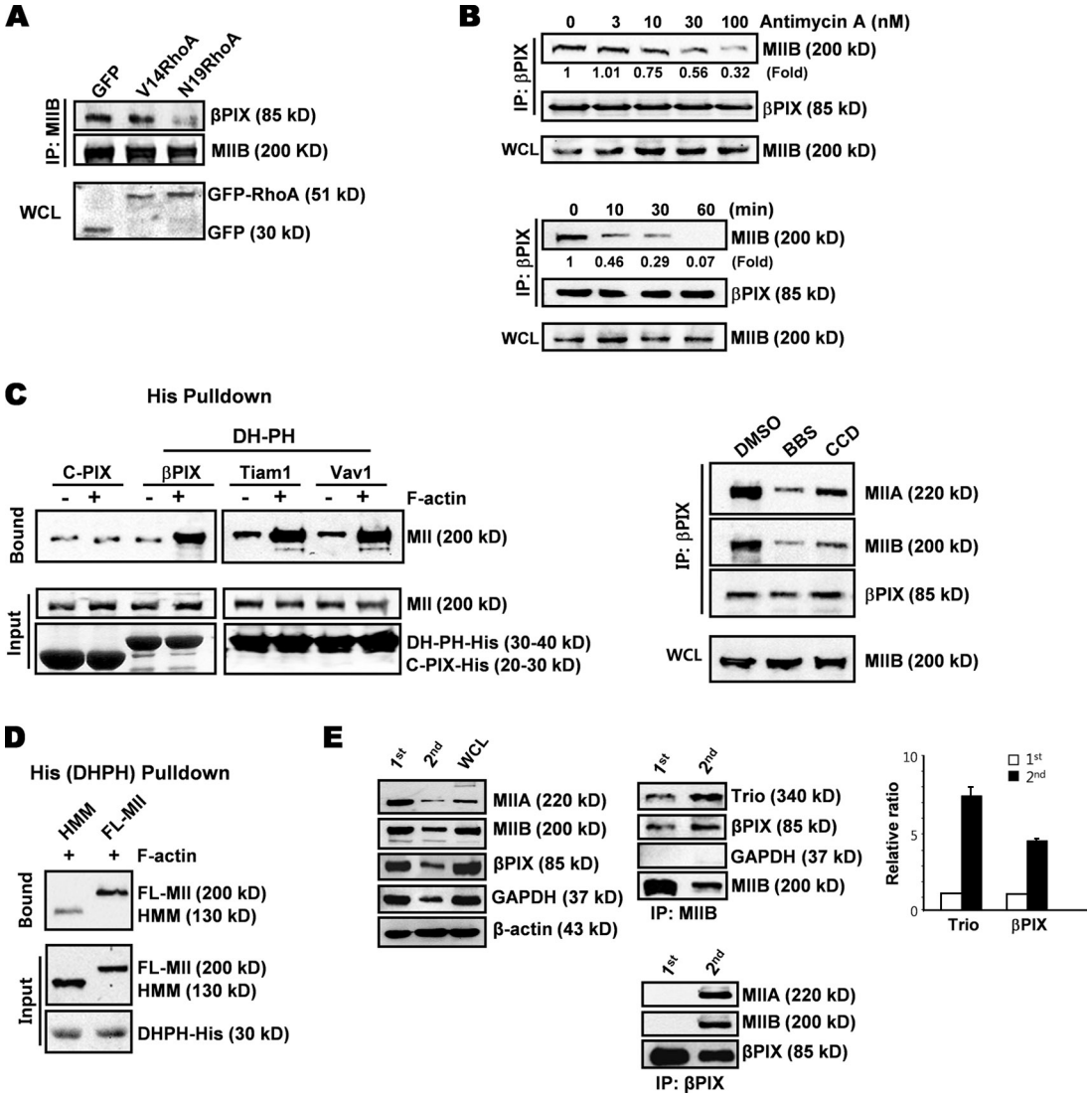

Figure 4. **Stimulation of MII–GEF association by MLC phosphorylation and actomyosin assembly.** (A) Inhibition of RhoA dissociates the MIIB–βPIX complex. 293T cells were transfected with the GFP control plasmid, dominant-active V14RhoA, or dominant-negative N19RhoA. The next day, lysates were immunoprecipitated with anti-MIIB antibody followed by immunoblotting for βPIX (top) or MIIB (bottom) (top). Expression of transfected genes was monitored by immunoblotting for GFP (bottom). (B) ATP depletion dissociates the MIIB–βPIX complex. (Top) NIH3T3 cells were incubated with depletion medium containing the indicated concentrations of antimycin A for 30 min. Lysates were immunoprecipitated with anti-βPIX and subjected to immunoblotting. (Bottom) Cells were treated with antimycin A (100 nM) for the indicated times. Lysates were processed as described above. Bound MIIB was analyzed by densitometry and the results are expressed relative to antimycin A–untreated controls. (C) F-actin stimulates association of the MIIB–DH–PH complex in vitro. (Left) 2 μg full-length skeletal muscle MII was incubated with 5 μg His-tagged C-PIX (negative control) or 5 μg DH–PH domains from βPIX, Tiam1, or Vav1 in the absence or presence of 0.2 mg/ml F-actin. MII–DH–PH complex was pulled down using Ni^{2+} beads. Bound MII was monitored by immunoblotting for muscle MII. (Right) Cells were incubated with DMSO, BBS (50 μM), or cytochalasin D (CCD, 10 μM) for 30 min. Lysates were immunoprecipitated with anti-βPIX and immunoblotted for MIIA or MIIB. (D) Thick filament assembly-dependent association of MII and DH–PH domain in vitro. HMM and full-length MII were incubated with the DH–PH domains from βPIX in the presence of F-actin. The complex was pulled down using Ni^{2+} beads, and bound HMM and MII were detected by immunoblotting for MII. Blots are representative of three independent experiments. (E) Assembly-dependent association of MII and GEFs in cells. (Left) NIH3T3 cells were extracted with mild, cytoskeleton stabilizing buffer conditions (first extract) and pellets then extracted with harsher buffer that solubilizes assembled myosin (second extract; Sandquist and Means, 2008). Distribution of MIIA, MIIB, βPIX, GAPDH, and β-actin in these fractions was monitored by immunoblotting. (Center) Both fractions were immunoprecipitated with anti-MIIB or anti-βPIX antibody followed by immunoblotting for βPIX, Trio, GAPDH, MIIA, or MIIB. (Right) Densitometry was performed on blots from three independent experiments. MIIB-bound GEFs were normalized to the immunoprecipitated amount of MIIB. The normalized value of each GEF for the first fraction was arbitrarily set to 1 and the relative ratio for the second faction was indicated. Bar graphs represent the mean ± SEM.

IP with anti-MIIB antibody and Western blotting. When normalized to the amount of MIIB in the IPs, the amount of βPIX and Trio was four- to sevenfold higher for assembled MIIB compared with the soluble pool (Fig. 4 E, center and right). GAPDH was present in both fractions (Fig. 4 E, left), and thus was used as a negative control. It did not coimmunoprecipitate with MIIB (Fig. 4 E, top center). In the reciprocal coIP experiment, βPIX associated mainly with MIIA and MIIB in the second assembled pool (Fig. 4 E, bottom center). Longer exposure revealed a weak association in the first soluble pool. These results support the idea that GEFs bind preferentially to assembled F-actin and MII filaments.

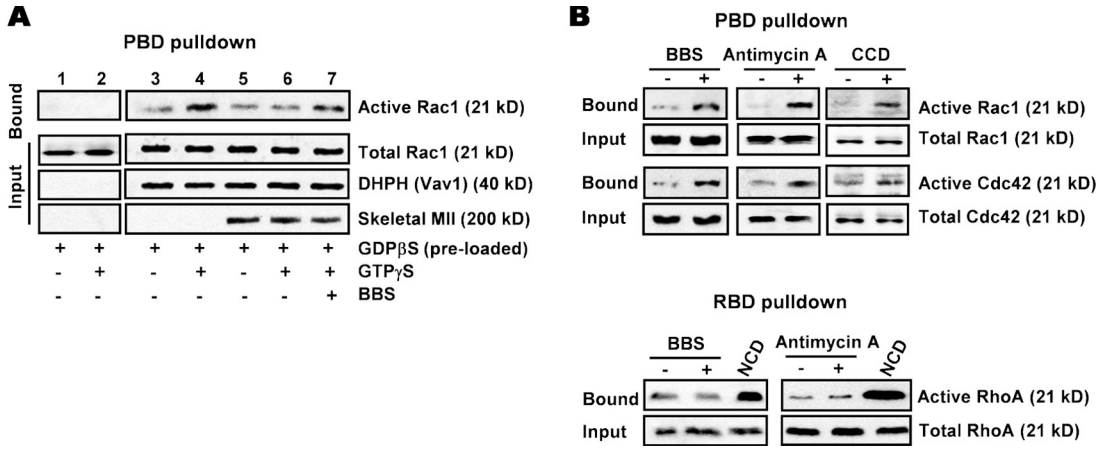

Figure 5. **Suppression of GEF activity by MII.** (A) Suppression of GEF activity by MII in vitro. GEF activity of recombinant His-tagged DH–PH domain of Vav1 expressed in *E. coli* toward Rac1 was measured in the absence (lanes 1–4) or presence (lanes 5 and 6) of MII or with BBS (50 μM) for 30 min (lane 7). (B) Suppression of GEF activity by MII in cells. (Top) NIH3T3 cells were treated with BBS (50 μM), antimycin A (100 nM), or cytochalasin D (10 μM) for 30 min. Rac1/Cdc42 activation was assessed using GST-PBD pull-down assays as described in Materials and methods. (Bottom) RhoA activation was assessed using the GST-RBD pull-down assay. NCD, nocodazole. Blots are representative from three independent experiments.

Dbl family GEFs are catalytically inactive when complexed with MII

As the catalytic DH–(PH) domain was shown to be MII binding site, we investigated the effects of MII binding on GEF activity. His-tagged DH–PH constructs were incubated with skeletal MII in vitro in the presence of GTPases and GTP. GEF activities were then measured using the p21-binding domain (PBD) pull-down assay (Benard et al., 1999). The Vav1 DH–PH domain alone showed high GEF activity toward Rac1 (Fig. 5 A, top, lanes 1–4), which was strongly inhibited by incubation with MII (compare lanes 4 and 6). DH–PH domains from Tiam1 and Dbs were similarly affected (not depicted). We further asked whether the suppressed GEF activity by bound MII could be reactivated by treatment with BBS that dissociates GEFs from MII (Fig. 3, A and B). Blebbistatin treatment indeed reactivated the GEF activity (compare lanes 6 and 7). To test whether the full-length GEFs in cells were inhibited by binding MII, cells were treated with BBS, cytochalasin D, or antimycin A to release GEFs from MII. The lysates were then subjected to a pull-down assay for measurement of Rac1, Cdc42, and RhoA activities. All these treatments caused activation of both Rac1 and Cdc42 (Fig. 5 B, top). In accordance with our results, these GTPases are also activated by treatment with ML-7 or Y-27632 (Katsumi et al., 2002; Grewal et al., 2008), which also reduced MII binding to GEFs (Fig. S2, A and B). No significant changes in RhoA activity were detected (Fig. 5 B, bottom), though nocodazole treatment induced a marked RhoA activation, as previously reported (Ren et al., 1999; Krendel et al., 2002; Chang et al., 2008). Together, these results support the idea that binding of MII inhibits GEF activity toward Rac1 and Cdc42.

BBS-induced release and activation of GEFs may be responsible for alteration in cell protrusion and adhesion

BBS and other inhibitors of MII induce membrane ruffling and activation of Rac and Cdc42 in multiple cell types (Katsumi et al., 2002; Loudon et al., 2006; Ryu et al., 2006; Even-Ram et al., 2007; Vicente-Manzanares et al., 2007). We therefore tested whether BBS-induced release of GEFs from MII mediated these events in cells. βPIX is a prominent GEF in fibroblasts (Cau and Hall, 2005); thus, we assessed this GEF in NIH3T3 cells. CoIP showed almost complete dissociation of βPIX from MIIA/IIB 30 min after BBS treatment (Fig. S4 A). Staining of cells after BBS treatment showed an irregular and diffuse staining of MIIA/IIB, and loss of stress fibers and increased lamellipodia (Fig. S4 B). βPIX became localized to a linear array of small puncta along the lamellipodia, previously described as focal complexes (Manser et al., 1998). To examine whether release of βPIX mediates the change in cell morphology, this protein was depleted using siRNA. βPIX knockdown reached 70–80%, as monitored by Western blotting (Fig. 6 A, bottom left) and fluorescence intensity (Fig. 6 A, top right). In scrambled siRNA-treated cells without BBS, vinculin localized to large focal adhesions at the cell periphery that overlapped with βPIX (Fig. 6 A, top left). BBS treatment caused a dramatic shift from large adhesions to numerous small focal complexes at the cell margin. βPIX siRNA had little effect on its own (Fig. 6 A, top right), but diminished the effect of BBS treatment by ∼50% (Fig. 6 A, bottom right). The increase in lamellipodia was also blocked (Fig. 6 B, top left); in fact, βPIX knockdown converted the BBS-induced increase to a decrease (Fig. 6 B, bottom). Collectively, these data suggest that BBS-induced release of βPIX leads to activation of Rac1, which induces lamellipodia and focal complexes.

PDGF induces transient dissociation of MII and βPIX by inactivating MII

BBS or antimycin A treatment inactivates MII, which results in release of GEFs and activation of Rac1/Cdc42. If this process is physiologically relevant, it should occur in response to physiological stimuli. PDGF potently stimulates fibroblast motility, which involves disassembly of focal adhesions and actin stress fibers and activation of Rac1 (Herman and Pledger, 1985; Greenwood et al., 2000; Jiménez et al., 2000). To test whether PDGF causes dissociation of the MII–GEF complex before Rac1

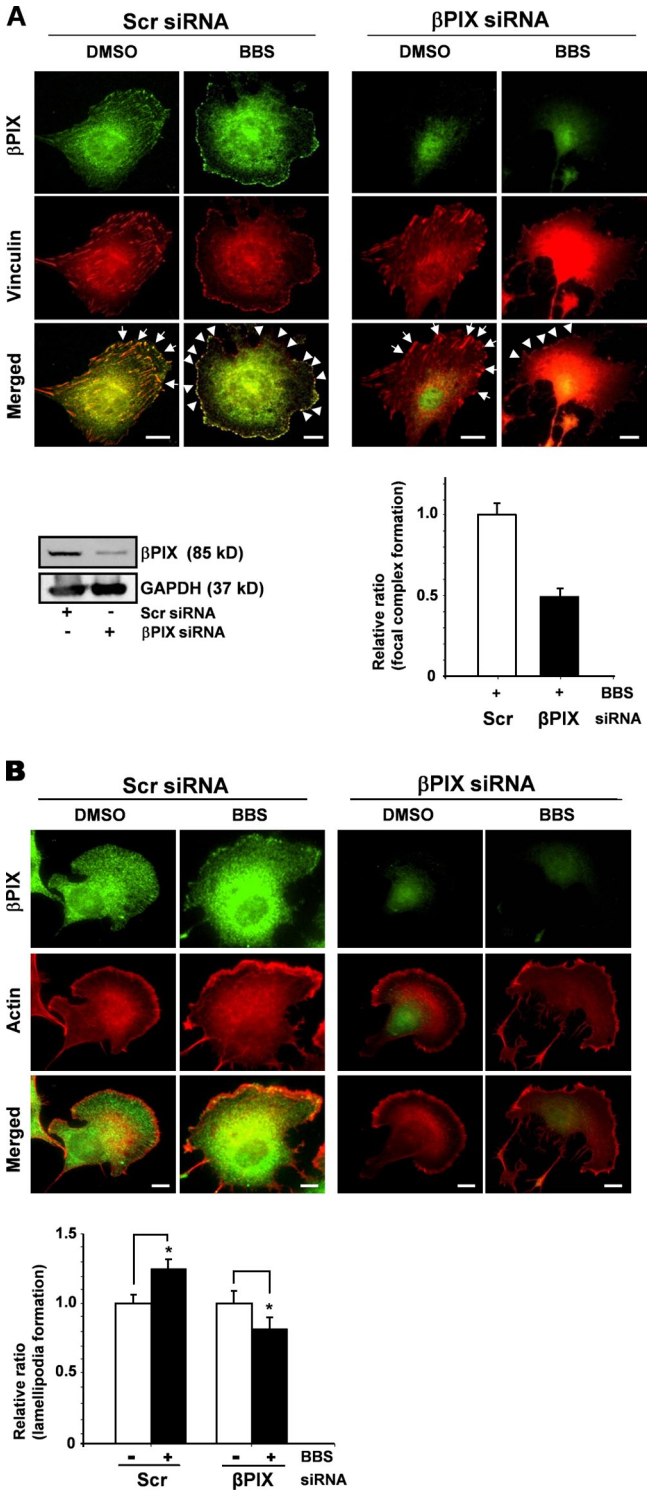

Figure 6. **Requirement for βPIX in MII-regulated cell protrusion and adhesion.** (A) βPIX mediates BBS-induced focal complex formation. Cells were treated with scrambled siRNA (Scr) or βPIX-specific siRNA for 2 d and then treated with DMSO or BBS for 30 min. (Top) Cells were fixed and stained for βPIX (green) and vinculin (red). Merged images are shown at the bottom. Bar, 10 µm. (Bottom) Knockdowns were monitored by immunoblotting (left). To quantify focal complex formation, we calculated the relative ratio, as defined in Materials and methods (right). The value of the relative ratio in control siRNA-treated cells (n = 29) was set to 1 and compared with that from βPIX siRNA-treated cells (n = 26). Quantitative data are expressed as means ± SEM. Note transformation of focal adhesions (arrows) to focal complexes (arrowheads) by BBS. (B) βPIX mediates BBS-induced lamellipodial protrusion. (Top) Cells were treated as described in A and stained for βPIX (green) and actin (red). (Bottom) To quantify lamellipodia formation, the relative ratio as defined in Materials and methods was obtained from each group of four. The values of the relative ratio in the two DMSO-treated groups (n = 48 for Scr siRNA; n = 36 for βPIX siRNA) were arbitrarily set to 1 and compared with those from the paired BBS-treated groups (n = 31 for Scr siRNA; n = 27 for βPIX siRNA). Values are means ± SEM. *, $P < 0.05$.

activation, NIH3T3 cells were stimulated with PDGF, then lysed and βPIX immunoprecipitated. Western blotting for MIIA and MIIB showed that PDGF treatment disrupted the complexes between MII isoforms and βPIX at 10–20 min after PDGF stimulation, followed by reformation at 30 min (Fig. 7 A, left). Dissociation of the MIIB–βPIX complex was dose dependent with maximum effects at 50 ng/ml of PDGF (Fig. 7 A, right). Subsequent experiments used this PDGF concentration for stimulation.

We next addressed whether MII inactivation was responsible for the transient release of GEFs from MII. Comparison of the time courses for PDGF-induced changes in actin cytoskeleton and focal adhesions (Herman and Pledger, 1985; Greenwood et al., 2000) to dissociation of the MII–GEF complexes (Fig. 7 A) was consistent with a causal role for MII inactivation in MII–GEF dissociation. As a functional test of this idea, the MLC mutants, MLC^{AA} and MLC^{EE}, in which Ser1/Ser2 and Thr18/Ser19 were replaced by alanines and glutamic acids, respectively, were prepared. These mutants have been demonstrated to incorporate into MII as well as wild-type MLC (MLC^{WT}) and confer resistance to PDGF-induced disassembly of stress fibers (Amano et al., 1998; Totsukawa et al., 2004; Komatsu and Ikebe, 2007). Lysates from cells expressing wild-type or mutant MLC were immunoprecipitated with anti-βPIX antibody and subjected to immunoblotting with anti-MIIB antibody. PDGF treatment dissociated MII and βPIX in vector or wild-type MLC-transfected cells, but MLC^{AA} or MLC^{EE} expression blocked this effect (Fig. 7 B). This effect was further analyzed by immunofluorescence. Before PDGF treatment, MLC and βPIX stained mainly stress fibers and some cortical actin structures (Fig. 7 C, left). Their colocalization was most apparent along the stress fibers. PDGF treatment triggered loss of stress fibers and more diffuse βPIX staining. Mutant MLC^{AA} or MLC^{EE} in untreated cells resembled wild-type MLC (Fig. 7 C, center and right); however, cells expressing these mutants were largely resistant to PDGF stimulation. Importantly, βPIX in these cells remained colocalized on stress fibers. Trio gave very similar results (Fig. S5). The collective results support the model that PDGF-induced MII inactivation leads to the dissociation of MII–GEF complex.

Because Rac1 and Cdc42 were strongly activated by the stimuli that released GEFs from MII (Fig. 5 B), we sought to determine whether PDGF-induced release of GEFs also stimulated these GTPases. A transient wave of Rac1 activation was observed within 2 min after PDGF treatment (Fig. 7 D, top), followed by a second wave of Rac1 activation at 30–40 min that gradually decreased. No noticeable Cdc42 activation was observed (unpublished data). Because the second wave of Rac1 activation corresponded to the release of GEFs from myosin, we tested whether blocking GEF release with active MLC^{EE} eliminated the second wave. Cells expressing MLC^{WT} showed two waves of Rac1

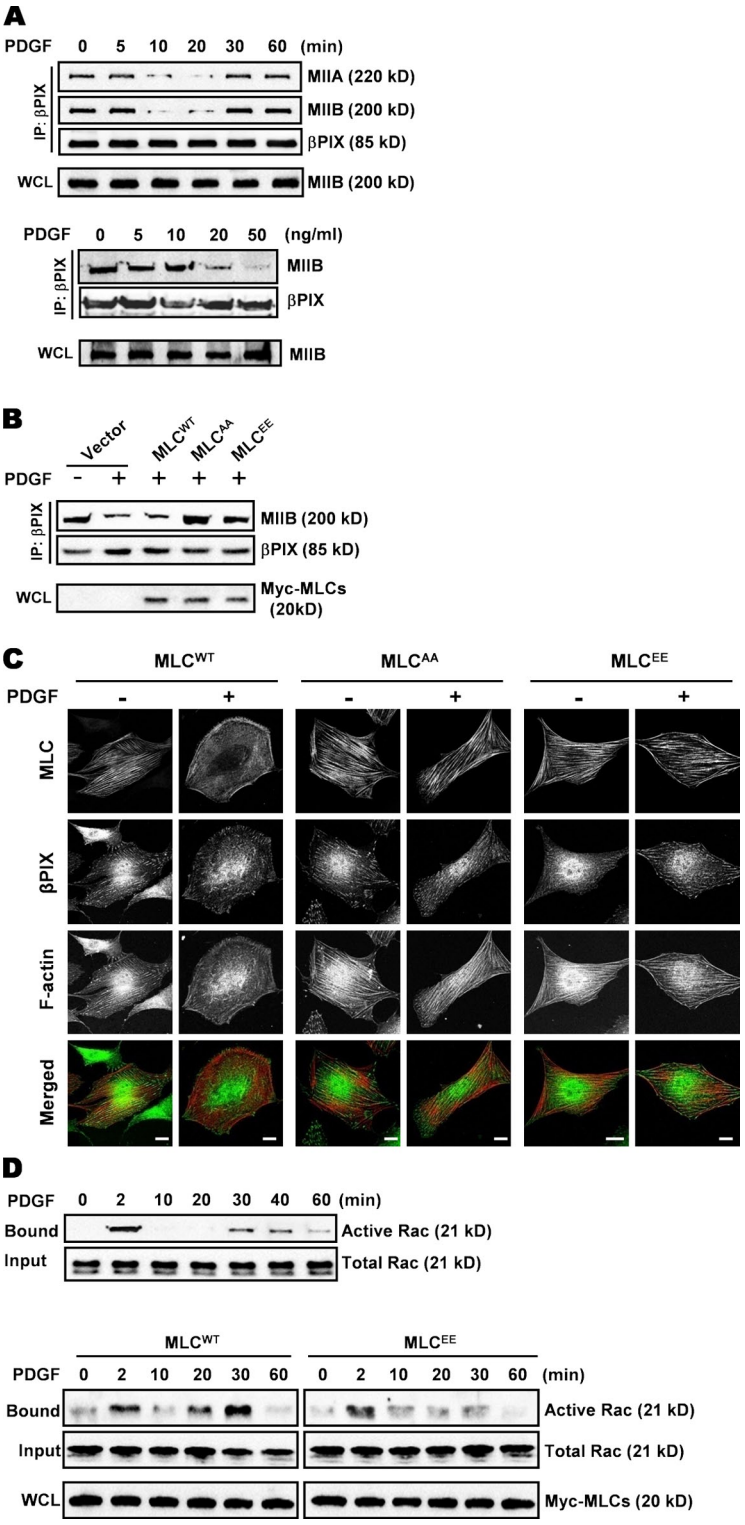

Figure 7. **PDGF-induced dissociation of the MII–βPIX complex.** (A) PDGF transiently dissociates the MII–βPIX complex. (Top) NIH3T3 cells were serum starved overnight and treated with 50 ng/ml PDGF for the indicated times. Lysates were immunoprecipitated with anti-βPIX antibody followed by immunoblotting for MIIA or MIIB. (Bottom) Cells were treated for 20 min with the indicated concentrations of PDGF. Lysates were immunoprecipitated with anti-βPIX antibody followed by immunoblotting for MIIB. (B) MLC mutants block PDGF-induced dissociation of the MIIB–βPIX complex. Cells were transfected with myc-tagged wild-type MLC (MLC^{WT}), MLC^{AA} (S1A/S2A), or MLC^{EE} (T18E/S19E). After 2 d, cells were treated with 50 ng/ml PDGF for 20 min. Lysates were immunoprecipitated with anti-βPIX antibody and immunoblotted for MIIB or βPIX. (C) Co-staining for βPIX and MLC mutants. Cells were transfected with myc-tagged MLC^{WT} (left), MLC^{AA} (center), or MLC^{EE} (right). After 1 d, cells were replated onto fibronectin-coated coverslips for 16 h, then treated with PDGF for 20 min. They were then fixed and stained for MLC (green), βPIX (red), and F-actin with Alexa Fluor 350–conjugated phalloidin. Bar, 10 μm. (D) PDGF stimulates biphasic Rac1 activation. Cells were treated with 50 ng/ml PDGF for the indicated times. Rac1 activation was assessed using a GST-PBD pull-down assay in nontransfected (top) and MLC-transfected cells (bottom). Data are representative of three independent experiments.

activation in response to PDGF stimulation, even though the second wave appeared earlier than in untransfected cells (Fig. 7 D, bottom left). In contrast, expression of MLC^{EE} completely suppressed only the second peak, while having no effect on the first peak of Rac activity (Fig. 7 D, bottom right). These results support the notion that MII inactivation–induced release of GEFs and their subsequent activation mediates Rho GTPase activation after PDGF treatment.

Discussion

Cell migration is an integrated process in which protrusion, adhesion and contraction are coordinated (Lauffenburger and Horwitz, 1996; Mitchison and Cramer, 1996). It is well established that Rho GTPases control MII contractility by modulating MLC/MHC phosphorylation. Conversely, MII controls Rho GTPases, as inhibition of MII by multiple means activates

Rac1/Cdc42 and downstream events. Recent studies suggested a possibility for Rho GTPase regulation by MII via the Dbl family of GEFs (Wu et al., 2006; Conti and Adelstein, 2008), but its mechanism was not determined. In the present study, we showed that MII bound a variety of Dbl family proteins with submicromolar affinity. Binding occurred through the head domain of myosin and the DH–PH region of the GEFs. This interaction increased upon myosin activation and blocked GEF activity toward Rac. Accordingly, myosin inactivation in cells triggered release of GEFs, leading to activation of Rac and Cdc42 and changes in cytoskeletal organization. These data therefore may provide a novel molecular mechanism for a variety of observations in which inhibition or removal of MII leads to lamellipodia formation, changes in cell adhesions, and increased cell motility (Katsumi et al., 2002; Sandquist et al., 2006; Even-Ram et al., 2007; Vicente-Manzanares et al., 2007).

MII showed substantial association with a surprising number of Dbl family GEFs, perhaps consistent with its interaction with the conserved DH–PH module. This result may imply that the interaction is mediated by conserved residues in the DH domains. Despite their structural and functional homology, sequence homology between different Rac and Cdc42 GEFs is often as low as 20% (Schmidt and Hall, 2002). It will therefore be interesting to further map the residues responsible for myosin binding and determine the relationship to myosin-dependent GTPase activation. Furthermore, although our collective data suggest a relatively general interaction between MII and GEFs, their functional contributions should be assessed with caution. For instance, the RhoA-specific GEF-H1 was released from MII upon treatment with BBS or antimycin A but RhoA activation was not observed. Suppression of Rho by more robust or faster activation of Rac/Cdc42 provides one possible explanation, but further work is required to fully understand the specificity for Rac and Cdc42.

We identified PDGF stimulation as one physiological system where this mechanism comes into play. PDGF is well known to induce myosin inactivation (Sander et al., 1999; Komatsu and Ikebe, 2007). We observed that PDGF triggered transient dissociation of GEFs from MII after MII inactivation, which correlated with a late wave of Rac1 activation. Importantly, phosphomimetic constitutively active MLC mutants abrogated PDGF-stimulated release of GEFs and activation of Rac. Our collective data therefore point to MII inactivation as an upstream event in PDGF-induced dissociation of the MII–GEF complex. The resultant Rac1 activation may further inactivate MII, thus forming a positive feedback loop, which contributes to persistence of directional migration.

Our data show that multiple nonmuscle and muscle isoforms of MII bind Rho family GEFs, indicating that it is a conserved function. However, quantitative differences in affinity were noted. It will therefore be interesting to test whether these differences in affinities for GEFs contribute to the functional differences between myosin isoforms. Thus, the distinct roles of MIIA and MIIB in cell migration may depend on different affinities for GEFs, as well as their different cellular locations and dynamics of assembly and disassembly (Even-Ram et al., 2007; Sandquist and Means, 2008). Understanding how the temporal and spatial aspects of these processes regulate cell motility will be an important direction for future research.

Cell motility is driven by an alternating process of actin polymerization–dependent protrusion and MII-dependent contraction. The molecular mechanism for coordination of these two processes is incompletely understood. We propose a novel role for MII as a regulator of Dbl family GEFs in coordinating these processes. Assembled, contractile MII associates with Dbl family GEFs and inhibits their catalytic activity, thereby suppressing activation of Rac1 and Cdc42, and subsequent cytoskeletal remodeling including formation of protrusions. It is noteworthy that myosin-containing actin stress fibers are most prominent along quiescent regions of the cell edge toward the back and sides, and absent from protrusive regions (Kolega, 1998, 2006; Gupton and Waterman-Storer, 2006). Stimuli that cause myosin inactivation lead to release of GEFs and activation of Rac1/Cdc42 GTPases. We therefore speculate that cycling of myosin between assembled/contracted and disassembled/relaxed states may represent a spatiotemporal regulatory mechanism in cell migration.

In conclusion, we provide a potential molecular mechanism for GEF regulation by MII in cell protrusion and adhesion. As MII and GEFs are ubiquitously expressed, it is also conceivable that cross talk between MII and a specific GEF(s) may represent a general mechanism to regulate diverse actomyosin-based cellular activities such as cell adhesion and cytokinesis.

Materials and methods

Antibodies and reagents

Anti-myosin, Tiam1, Dbl, LARG, FGD1, and Trio antibodies were purchased from Santa Cruz Biotechnology, Inc. Anti-GEF-H1 and Vav1 antibodies were obtained from Cell Signaling Technology. Anti-kalirin antibody was purchased from Millipore. Anti-skeletal and cardiac muscle myosin antibodies were purchased from Abcam. Rabbit skeletal or cardiac muscle MII, HMM, and preformed F-actin were purchased from Cytoskeleton, Inc. Secondary Alexa Fluor 488–, 546–, 594–conjugated antibodies, Alexa Fluor 350–conjugated phalloidin, and βPIX siRNA (5′-TTGTCTATCAGGATGATA-ATCCTCC-3′) were purchased from Invitrogen. TRITC-conjugated phalloidin, PDGF, cytochalasin D, nocodazole, antimycin A, ML-7, and Y-27632 were obtained from Sigma-Aldrich. BBS was purchased from Tocris Bioscience. Sensor chip NTA and buffers for surface plasmon resonance binding assay were obtained from GE Healthcare.

Plasmid constructs

Full-length cDNAs were purchased from the following sources: human nonmuscle MIIB heavy chain (NMYH-IIB: MGC134913) from Addgene; collybistin, GEFT, intersectin, and myosin light chain (MLC) from American Type Culture Collection (Manassas, VA); PDZRhoGEF and smgGDS from Kazusa DNA Research Institute; and GEF-H1, FGD1, and ARNO from 21C Frontier Human Gene Bank (Daejeon, Korea). cDNAs for the βPIX DH/DH–PH domain (amino acid [aa] 100–276/100–400); the Tiam1 DH/DH–PH domain (aa 1048–1239/1048–1406); GEFT (aa 163–334/163–466); collybistin (aa 108–285/104–426); and Vav1 (aa 195–352/195–508) were subcloned into pCMV-myc (Takara Bio Inc.) or the pET-24a vector (EMD). The cDNA for N-PIX (aa 1–400), C-PIX (aa 401–647), and MLC were each subcloned into pCMV-myc (Takara Bio Inc.). The cDNA for Head (aa 1–843); Rod-1 (aa 844–1319); Rod-2 (aa 1320–1976); or HMM (aa 1–1045) for nonmuscle MIIB and HMM (aa 1 –1040) for nonmuscle MIIA were each subcloned into the pEGFP vector. Mutant constructs of HMM and MLC were generated using a QuikChange site-directed mutagenesis kit (Agilent Technologies) according to the manufacturer's protocol. The following primers were used for mutagenic polymerase chain reaction (PCR): HMM (MIIA): sense 5′-CTCACGTGCCTCAAAGAAGCCTCGGTGCTG-3′ and antisense 5′-CAGCACCGAGGCTTCTTTGAGGCACGTGAG-3′; for N93K, sense 5′-GTTCTCGAGGGCATCTGTATCTGCCGCCAG-3′ and antisense 5′-CTGGCGGCAGATACAGATGCCCTCGAGAAC-3′; for R702C:

HMM (MIIB): sense 5′-GAATTGACATGCTTGAAAGAAGCTTCCGTT-3′ and antisense 5′-AACGGAAGCTTCTTTCAAGCATGTCAATTC-3′; for N97K, sense 5′-GTCCTGGAAGGGATCTGCATCTGTCGCCAG-3′ and antisense 5′-CTGGCGACAGATGCAGATCCCTTCCAGGAC-3′; for R709C: MLC^{AA}: sense 5′-GTCGACCATGGCGGCCAAAAAGGCAAAGAC-3′ and antisense 5′-GTCTTGCCTTTTTGGCCGCCATGGTCGAC-3′; for MLC^{EE}: sense 5′-CCTCAGCGTGCAGAAGAGAATGTGTTTGCCATG-3′ and antisense 5′-GGCAAACACATTCTCTTCTGCACGCTGAGG-3′.

Cell culture and transfection

NIH3T3, Swiss 3T3, 293T, C2C12, and PC12 cells were cultured in DME (Invitrogen) and Jurkat T cells were cultured in RPMI1640 (Invitrogen) supplemented with 10% fetal bovine serum and 100 U/ml penicillin/streptomycin (Invitrogen) at 37°C in a humidified 5% CO_2 incubator. For the ATP depletion study, cells were cultured in the depletion medium containing indicated concentrations of antimycin A for 30 min (Canfield et al., 1991). For transfections, cells in 60-mm-diameter dishes or on fibronectin-coated coverslips were incubated with a mixture of DNA and LipofectAMINE 2000 (Invitrogen) according to the manufacturer's instructions. Cells were used 24–48 h after transfection.

Fluorescence microscopy

Cells were fixed using 3.7% paraformaldehyde in PBS for 15 min, permeabilized using 0.2% Triton X-100 in PBS for 2 min, blocked with 2% BSA in PBS, and stained with the indicated primary antibodies for at 4°C overnight, followed by incubation with a secondary Alexa Fluor 488–, 546– or 594–conjugated antibody. F-actin was visualized with TRITC or Alexa Fluor 350–conjugated phalloidin. Cells were imaged on a laser confocal microscope (LSM 710; Carl Zeiss, Inc.) with a Plan Apochromat 63x objective (Carl Zeiss, Inc.). Alterations in cell adhesion/protrusion were visualized under an inverted microscope (IX81-ZDC; Olympus) with a PlanApo N 60x objective (Olympus). To quantify adhesions, cells were double labeled with βPIX and vinculin. Both the total cell perimeter and the portion of the perimeter occupied by the focal complexes were measured using MetaMorph software version 7.1.7 (MDS Analytical Technologies). The relative ratio of focal complex formation was defined as the perimeter occupied by the focal complexes divided by total cell perimeter. To quantify lamellipodial protrusion after BBS treatment, cells were co-stained for βPIX and actin. The relative ratio of lamellipodia formation was defined as the perimeter occupied by the lamellipodia divided by total cell perimeter.

Immunoprecipitation and immunoblotting

Rat brain (E18) and cells were lysed in cold lysis buffer containing 50 mM Hepes, pH 7.5, 150 mM NaCl, 1 mM NaF, 10% glycerol, 1% Triton X-100, 200 µM orthovanadate, and protease inhibitor cocktail. Cell lysates were immunoprecipitated with indicated antibodies for 3 h at 4°C. Immunoprecipitates were collected by adding protein A– or G–Sepharose for 3 h at 4°C, and washed five times with lysis buffer. Samples were resolved by SDS-PAGE, and transferred to a polyvinylidene difluoride membrane in a Tris-glycine methanol buffer (25 mM Tris base, 200 mM glycine, and 20% methanol). Membranes were blocked with 3% skimmed milk in phosphate-buffered saline (PBS) containing 0.1% Tween 20 (PBST) for 30 min, incubated with primary antibodies for 1 h, and washed three times with PBST. Membranes were blotted with secondary HRP-conjugated antibodies for 1 h. After five washes with PBST, signals were detected using enhanced chemiluminescence (ECL) reagent (GE Healthcare). In some cases, membranes were stripped and reprobed with different antibodies (Shin et al., 2004). To quantify MII-bound GEFs, densitometry was performed using Quantity One software version 4.6.7 (Bio-Rad Laboratories).

Fractionation for soluble and assembled myosin II

NIH3T3 cells were extracted in situ with cytoskeleton stabilization buffer (10 mM Pipes, pH 6.8, 50 mM NaCl, 2.5 mM $MgCl_2$, 1 mM EGTA, 0.3 M sucrose, 0.5% Triton X-100, and protease inhibitor cocktail) for 5 min on ice. The supernatant was retrieved as the first fraction, which contains soluble MII. The remaining, attached material containing assembled myosin was extracted with standard lysis buffer (50 mM Hepes, pH 7.5, 150 mM NaCl, 100 mM NaF, 10% glycerol, 1% Triton X-100, 200 µM orthovanadate, and protease inhibitor cocktail). The lysates were centrifuged at 16,000 *g* for 15 min and the supernatant was used as the second fraction. Both fractions were immunoprecipitated with anti-MIIB or anti-βPIX antibody followed by immunoblotting for Trio, βPIX, MIIA, MIIB, or GAPDH. Blots were quantified by densitometry using Quantity One software version 4.6.7.

Pull-down assay

To investigate the direct binding between the MII and DH–PH domain (Fig. 2 D), muscle MII (2 µg) was incubated with purified GST-tagged DH–PH domains (5 µg) in binding buffer (15 mM Tris HCl, pH 7.5, 2.5 mM $MgCl_2$, 0.1 mM EGTA, and 0.05% Triton X-100) at 25°C for 30 min. The mixture was then pulled down by glutathione agarose beads. To analyze the effect of F-actin on the binding between MII and His-tagged DH–PH domain (Fig. 4 C), they were incubated in the absence or presence of 0.2 mg/ml preformed F-actin in binding buffer at 25°C for 1 h. The MII–DH–PH complex was pulled down using Ni^{2+} beads. Pull-down assays to test the effect of MII on the GEF activity of the DH–PH domain in vitro used His-DH–PH (2 µg) and His-Rac1 (2 µg) preloaded with 1 mM GDPβS. They were incubated with or without skeletal muscle MII for 30 min, and with or without BBS (50 µM). These mixtures were then incubated with 100 µM GTPγS at 25°C for 30 min to allow GTPase activation. Active Rac1 was pulled down with GST-PBD (p21 binding domain) and analyzed by immunoblotting for Rac1 (Benard et al., 1999). For cell experiments, NIH3T3 cells were treated with 50 µM BBS, 100 nM antimycin A, 10 µM cytochalasin D, or 10 µM nocodazole for 30 min (Fig. 5 B). Active Rac1, Cdc42, or RhoA in the lysates was pulled down by GST-PBD or GST-RBD (Rhotekin binding domain; Ren et al., 1999).

Surface plasmon resonance binding assay

Kinetic analysis of the interaction of DH–PH domains and skeletal muscle MII used a BIAcore 2000 instrument (Biacore). Sensor NTA chips (GE Healthcare) were loaded with 0.5 mM nickel sulfate in running buffer (10 mM Hepes, pH 7.4, 150 mM NaCl, 50 µM EDTA, and 0.005% Surfactant P20) and incubated with purified His-tagged DH–PH domains from βPIX, Vav1, or Tiam1 and the C-terminal half of βPIX (C-PIX) as a negative control at a flow rate of 10 µl/min until recording a signal of ∼8,000 response units (RU). Various concentrations of skeletal muscle MII were then injected into the flow cells at a flow rate of 20 µl/min. Specific binding of MII with DH–PH domain was obtained by subtracting nonspecific binding of MII with C-PIX. The equilibrium dissociation constant (Kd = kd/ka) was derived from the calculated dissociation rate constant (kd) and the association rate constant (ka) using BIAevaluation software, version 3.0.2 (GE Healthcare). Kinetic data fitted to the 1:1 binding model with a drifting baseline.

Statistical analysis

Paired *t* tests were performed using SPSS version 10.0 for Windows (SPSS) and the statistical significance was set at $P < 0.05$.

Online supplemental material

Fig. S1 shows colocalization of exogenously introduced βPIX (myc-βPIX) and MIIs in Swiss 3T3 fibroblasts. Fig. S2 shows colocalization of endogenous βPIX/Trio and MIIs in NIH3T3 fibroblasts. Fig. S3 shows dissociation of the MII–GEF complex by treatment with ML-7, Y-27632, or antimycin A. Fig. S4 shows BBS-induced dissociation of the MII–βPIX complex and alterations in βPIX staining in NIH3T3 cells. Fig. S5 shows that expression of active MLC mutants (MLC^{AA} or MLC^{EE}) inhibits the dissociation of MII–Trio complex. Online supplemental material is available at http://www.jcb.org/cgi/content/full/jcb.201003057/DC1.

We gratefully acknowledge those who provided cDNA: Dr. X.M. Ma (University of Connecticut Health Center), Dr. J.G. Collard (The Netherlands Cancer Institute), and Dr. Y.S. Bae (Ewha Womans University).

This research was supported, in part, by Basic Science Research Program through the National Research Foundation of Korea (NRF) funded by the Ministry of Education, Science and Technology (2010-0001271) and USPHS grant RO1 GM47214 to M.A. Schwartz.

Submitted: 12 March 2010
Accepted: 27 July 2010

References

Adelstein, R.S., and M.A. Conti. 1975. Phosphorylation of platelet myosin increases actin-activated myosin ATPase activity. *Nature.* 256:597–598. doi:10.1038/256597a0

Amano, M., K. Chihara, N. Nakamura, Y. Fukata, T. Yano, M. Shibata, M. Ikebe, and K. Kaibuchi. 1998. Myosin II activation promotes neurite retraction during the action of Rho and Rho-kinase. *Genes Cells.* 3:177–188. doi:10.1046/j.1365-2443.1998.00181.x

Benard, V., B.P. Bohl, and G.M. Bokoch. 1999. Characterization of rac and cdc42 activation in chemoattractant-stimulated human neutrophils using a novel assay for active GTPases. *J. Biol. Chem.* 274:13198–13204. doi:10.1074/jbc.274.19.13198

Canfield, P.E., A.M. Geerdes, and B.A. Molitoris. 1991. Effect of reversible ATP depletion on tight-junction integrity in LLC-PK1 cells. *Am. J. Physiol.* 261:F1038–F1045.

Cau, J., and A. Hall. 2005. Cdc42 controls the polarity of the actin and microtubule cytoskeletons through two distinct signal transduction pathways. *J. Cell Sci.* 118:2579–2587. doi:10.1242/jcs.02385

Chang, Y.C., P. Nalbant, J. Birkenfeld, Z.F. Chang, and G.M. Bokoch. 2008. GEF-H1 couples nocodazole-induced microtubule disassembly to cell contractility via RhoA. *Mol. Biol. Cell.* 19:2147–2153. doi:10.1091/mbc.E07-12-1269

Choi, C.K., M. Vicente-Manzanares, J. Zareno, L.A. Whitmore, A. Mogilner, and A.R. Horwitz. 2008. Actin and alpha-actinin orchestrate the assembly and maturation of nascent adhesions in a myosin II motor-independent manner. *Nat. Cell Biol.* 10:1039–1050. doi:10.1038/ncb1763

Conti, M.A., and R.S. Adelstein. 2008. Nonmuscle myosin II moves in new directions. *J. Cell Sci.* 121:11–18. doi:10.1242/jcs.007112

Even-Ram, S., A.D. Doyle, M.A. Conti, K. Matsumoto, R.S. Adelstein, and K.M. Yamada. 2007. Myosin IIA regulates cell motility and actomyosin-microtubule crosstalk. *Nat. Cell Biol.* 9:299–309. doi:10.1038/ncb1540

Gallagher, P.J., B.P. Herring, S.A. Griffin, and J.T. Stull. 1991. Molecular characterization of a mammalian smooth muscle myosin light chain kinase. *J. Biol. Chem.* 266:23936–23944.

Greenwood, J.A., A.B. Theibert, G.D. Prestwich, and J.E. Murphy-Ullrich. 2000. Restructuring of focal adhesion plaques by PI 3-kinase. Regulation by PtdIns (3,4,5)-p(3) binding to alpha-actinin. *J. Cell Biol.* 150:627–642. doi:10.1083/jcb.150.3.627

Grewal, S., J.G. Carver, A.J. Ridley, and H.J. Mardon. 2008. Implantation of the human embryo requires Rac1-dependent endometrial stromal cell migration. *Proc. Natl. Acad. Sci. USA.* 105:16189–16194. doi:10.1073/pnas.0806219105

Gupton, S.L., and C.M. Waterman-Storer. 2006. Spatiotemporal feedback between actomyosin and focal-adhesion systems optimizes rapid cell migration. *Cell.* 125:1361–1374. doi:10.1016/j.cell.2006.05.029

Herman, B., and W.J. Pledger. 1985. Platelet-derived growth factor-induced alterations in vinculin and actin distribution in BALB/c-3T3 cells. *J. Cell Biol.* 100:1031–1040. doi:10.1083/jcb.100.4.1031

Hu, A., F. Wang, and J.R. Sellers. 2002. Mutations in human nonmuscle myosin IIA found in patients with May-Hegglin anomaly and Fechtner syndrome result in impaired enzymatic function. *J. Biol. Chem.* 277:46512–46517. doi:10.1074/jbc.M208506200

Jiménez, C., R.A. Portela, M. Mellado, J.M. Rodríguez-Frade, J. Collard, A. Serrano, C. Martínez-A, J. Avila, and A.C. Carrera. 2000. Role of the PI3K regulatory subunit in the control of actin organization and cell migration. *J. Cell Biol.* 151:249–262. doi:10.1083/jcb.151.2.249

Katsumi, A., J. Milanini, W.B. Kiosses, M.A. del Pozo, R. Kaunas, S. Chien, K.M. Hahn, and M.A. Schwartz. 2002. Effects of cell tension on the small GTPase Rac. *J. Cell Biol.* 158:153–164. doi:10.1083/jcb.200201105

Kim, K.Y., M. Kovács, S. Kawamoto, J.R. Sellers, and R.S. Adelstein. 2005. Disease-associated mutations and alternative splicing alter the enzymatic and motile activity of nonmuscle myosins II-B and II-C. *J. Biol. Chem.* 280:22769–22775. doi:10.1074/jbc.M503488200

Kolega, J. 1998. Cytoplasmic dynamics of myosin IIA and IIB: spatial 'sorting' of isoforms in locomoting cells. *J. Cell Sci.* 111:2085–2095.

Kolega, J. 2006. The role of myosin II motor activity in distributing myosin asymmetrically and coupling protrusive activity to cell translocation. *Mol. Biol. Cell.* 17:4435–4445. doi:10.1091/mbc.E06-05-0431

Komatsu, S., and M. Ikebe. 2007. The phosphorylation of myosin II at the Ser1 and Ser2 is critical for normal platelet-derived growth factor induced reorganization of myosin filaments. *Mol. Biol. Cell.* 18:5081–5090. doi:10.1091/mbc.E06-12-1076

Kovács, M., J. Tóth, C. Hetényi, A. Málnási-Csizmadia, and J.R. Sellers. 2004. Mechanism of blebbistatin inhibition of myosin II. *J. Biol. Chem.* 279:35557–35563. doi:10.1074/jbc.M405319200

Krendel, M., F.T. Zenke, and G.M. Bokoch. 2002. Nucleotide exchange factor GEF-H1 mediates cross-talk between microtubules and the actin cytoskeleton. *Nat. Cell Biol.* 4:294–301. doi:10.1038/ncb773

Lauffenburger, D.A., and A.F. Horwitz. 1996. Cell migration: a physically integrated molecular process. *Cell.* 84:359–369. doi:10.1016/S0092-8674(00)81280-5

Loudon, R.P., L.D. Silver, H.F. Yee Jr., and G. Gallo. 2006. RhoA-kinase and myosin II are required for the maintenance of growth cone polarity and guidance by nerve growth factor. *J. Neurobiol.* 66:847–867. doi:10.1002/neu.20258

Manser, E., T.H. Loo, C.G. Koh, Z.S. Zhao, X.Q. Chen, L. Tan, I. Tan, T. Leung, and L. Lim. 1998. PAK kinases are directly coupled to the PIX family of nucleotide exchange factors. *Mol. Cell.* 1:183–192. doi:10.1016/S1097-2765(00)80019-2

Mitchison, T.J., and L.P. Cramer. 1996. Actin-based cell motility and cell locomotion. *Cell.* 84:371–379. doi:10.1016/S0092-8674(00)81281-7

Nobes, C.D., and A. Hall. 1995. Rho, rac and cdc42 GTPases: regulators of actin structures, cell adhesion and motility. *Biochem. Soc. Trans.* 23:456–459.

Raman, N., and S.J. Atkinson. 1999. Rho controls actin cytoskeletal assembly in renal epithelial cells during ATP depletion and recovery. *Am. J. Physiol.* 276:C1312–C1324.

Ren, X.D., W.B. Kiosses, and M.A. Schwartz. 1999. Regulation of the small GTP-binding protein Rho by cell adhesion and the cytoskeleton. *EMBO J.* 18:578–585. doi:10.1093/emboj/18.3.578

Ryu, J., L. Liu, T.P. Wong, D.C. Wu, A. Burette, R. Weinberg, Y.T. Wang, and M. Sheng. 2006. A critical role for myosin IIb in dendritic spine morphology and synaptic function. *Neuron.* 49:175–182. doi:10.1016/j.neuron.2005.12.017

Sander, E.E., J.P. ten Klooster, S. van Delft, R.A. van der Kammen, and J.G. Collard. 1999. Rac downregulates Rho activity: reciprocal balance between both GTPases determines cellular morphology and migratory behavior. *J. Cell Biol.* 147:1009–1022. doi:10.1083/jcb.147.5.1009

Sandquist, J.C., and A.R. Means. 2008. The C-terminal tail region of nonmuscle myosin II directs isoform-specific distribution in migrating cells. *Mol. Biol. Cell.* 19:5156–5167. doi:10.1091/mbc.E08-05-0533

Sandquist, J.C., K.I. Swenson, K.A. Demali, K. Burridge, and A.R. Means. 2006. Rho kinase differentially regulates phosphorylation of nonmuscle myosin II isoforms A and B during cell rounding and migration. *J. Biol. Chem.* 281:35873–35883. doi:10.1074/jbc.M605343200

Schmidt, A., and A. Hall. 2002. Guanine nucleotide exchange factors for Rho GTPases: turning on the switch. *Genes Dev.* 16:1587–1609. doi:10.1101/gad.1003302

Shin, E.Y., K.N. Woo, C.S. Lee, S.H. Koo, Y.G. Kim, W.J. Kim, C.D. Bae, S.I. Chang, and E.G. Kim. 2004. Basic fibroblast growth factor stimulates activation of Rac1 through a p85 betaPIX phosphorylation-dependent pathway. *J. Biol. Chem.* 279:1994–2004. doi:10.1074/jbc.M307330200

Somlyo, A.P., and A.V. Somlyo. 2000. Signal transduction by G-proteins, rho-kinase and protein phosphatase to smooth muscle and non-muscle myosin II. *J. Physiol.* 522:177–185. doi:10.1111/j.1469-7793.2000.t01-2-00177.x

Straight, A.F., A. Cheung, J. Limouze, I. Chen, N.J. Westwood, J.R. Sellers, and T.J. Mitchison. 2003. Dissecting temporal and spatial control of cytokinesis with a myosin II inhibitor. *Science.* 299:1743–1747. doi:10.1126/science.1081412

Totsukawa, G., Y. Wu, Y. Sasaki, D.J. Hartshorne, Y. Yamakita, S. Yamashiro, and F. Matsumura. 2004. Distinct roles of MLCK and ROCK in the regulation of membrane protrusions and focal adhesion dynamics during cell migration of fibroblasts. *J. Cell Biol.* 164:427–439. doi:10.1083/jcb.200306172

Vicente-Manzanares, M., J. Zareno, L. Whitmore, C.K. Choi, and A.F. Horwitz. 2007. Regulation of protrusion, adhesion dynamics, and polarity by myosins IIA and IIB in migrating cells. *J. Cell Biol.* 176:573–580. doi:10.1083/jcb.200612043

Wu, D., M. Asiedu, R.S. Adelstein, and Q. Wei. 2006. A novel guanine nucleotide exchange factor MyoGEF is required for cytokinesis. *Cell Cycle.* 5:1234–1239.

Za, L., C. Albertinazzi, S. Paris, M. Gagliani, C. Tacchetti, and I. de Curtis. 2006. betaPIX controls cell motility and neurite extension by regulating the distribution of GIT1. *J. Cell Sci.* 119:2654–2666. doi:10.1242/jcs.02996